

SCIENTIFIC REPORTS



OPEN

Few Ramachandran Angle Changes Provide Interaction Strength Increase in A β 42 versus A β 40 Amyloid Fibrils

Oscar H. Bastidas, Benjamin Green, Mary Sprague & Michael H. Peters

Received: 15 August 2016

Accepted: 17 October 2016

Published: 03 November 2016

The pathology of Alzheimer's disease can ultimately be traced to the increased aggregation stability of A β 42 peptides which possess two extra residues (Ile 41 & Ala 42) that the non-pathological strain (A β 40) lacks. We have found A β 42 fibrils to exhibit stronger energies in inter-chain interactions and we have also identified the cause for this increase to be the result of different Ramachandran angle values in certain residues of the A β 42 strain compared to A β 40. These unique angle configurations result in the peptide planes in the fibril structures to be more vertical along the fibril axis for A β 42 which thus reduces the inter-atomic distance between interacting atoms on vicinal peptide chains thereby increasing the electrostatic interaction energies. We lastly postulate that these different Ramachandran angle values could possibly be traced to the unique conformational folding avenues sampled by the A β 42 peptide owing to the presence of its two extra residues.

The neurodegeneration that marks the onset of Alzheimer's disease (AD) is believed to be caused by neurotoxic soluble aggregate oligomers of A β 42 peptides that result from the cleavage of the Alzheimer precursor protein¹. In this disorder, A β 42 peptides co-exist with the more benign A β 40 peptide but at a greater A β 42/A β 40 ratio, where the A β 42 is much more pathogenic²⁻⁴. This has recently been demonstrated to be clinically significant as measurements of A β 42/A β 40 ratios in cerebrospinal fluid can function as an important clinical diagnostic marker of AD⁵. A β 42's pathogenicity is consequently owed to its greater neuronal toxicity, greater aggregation propensity, and its increased kinetics or rate of aggregate formation compared to A β 40⁶⁻¹⁰. Small, prefibrillar/oligomeric aggregate species of A β 42 are now recognized as the primary neurotoxic species responsible for neuronal death in Alzheimer's disease¹¹⁻¹⁵ although there is also a recognized appreciable toxicity of A β 42 mature fibrils as has been seen in cell culture experiments¹⁶⁻¹⁹. In this regard, mature fibril aggregates are also known to act as a source of these toxic pre-fibrillar oligomers and aggregates in aggregation pathway schemes²⁰⁻²². Neurotoxicity is thought to proceed by A β 42 targeting the synapse of neurons²³ with the likely mechanism of cell death being apoptosis²⁴.

Despite the obvious clinical importance of both oligomers and fibrils, their structural details at the atomic level have been unfortunately difficult to characterize^{12,25-28}. It is known, however, that in these aggregate species, the constituent peptide chains, or monomers, of both A β 40 and A β 42 are held together by hydrogen bonds that stabilize the aggregate formation²⁹⁻³¹. In spite of the enigmatic nature of A β 40 and A β 42 oligomeric structure, there is a recognized considerable difference in morphology between A β 40 and A β 42 aggregates as evidenced by aggregation seeds of one strain failing to initiate fibril formation in the other³²⁻³⁴. These differences in morphology have been observed in experimentally determined structures of A β 40 and A β 42 mature fibrils, which demonstrate distinct differences in both their conformations and size, or number of constituent monomer A β chains. The addition of only two residues, as seen in the A β 42 strain, significantly alters the folded state conformations of the monomer chains in the mature fibril structure. Such distinctions have even been proposed as clinically significant in their exploitation as potential novel biomarkers for diagnosing late phase Alzheimer's disease specifically exploiting the more β -sheet rich A β 42 isoform³⁵. A comparison of the structural and energetic properties of mature A β 40 and A β 42 fibrils may therefore provide insight into key differences between the two isoforms and thus help to establish the structural and energetic constraints on their fibril formation pathways.

Department of Chemical and Life Science Engineering, Virginia Commonwealth University, Richmond, Virginia, United States of America. Correspondence and requests for materials should be addressed to M.H.P. (email: mpeters@vcu.edu)

| | A β 40 (A-D) | A β 42 (A-B) |
|----------------------------------------|--------------------|--------------------|
| Coulombic Interactions: | 811 | 779 |
| Coulombic Average E (<i>kT</i>): | -0.729 \pm 0.006 | -0.819 \pm 0.008 |
| Coulombic Average D (nm): | 0.575 \pm 0.001 | 0.568 \pm 0.001 |
| Lennard-Jones Interactions: | 135 | 118 |
| Lennard-Jones Average E (<i>kT</i>): | -0.177 \pm 0.001 | -0.188 \pm 0.002 |
| Lennard-Jones Average D (nm) | 0.397 \pm 0.001 | 0.393 \pm 0.001 |

Table 1. Comparison of the quantity of the number of dominant atom-atom interaction pairs, average energy (per interaction pair) and average inter-atomic distance (per interaction pair) of 1:2 atom-atom interactions between two chains for A β 40 (A-D chain mapping results) and A β 42 (A-B chain mapping results) with 95% confidence intervals for analysis across all ensemble members. Energy units are in *kT* and distance units are in nanometers.

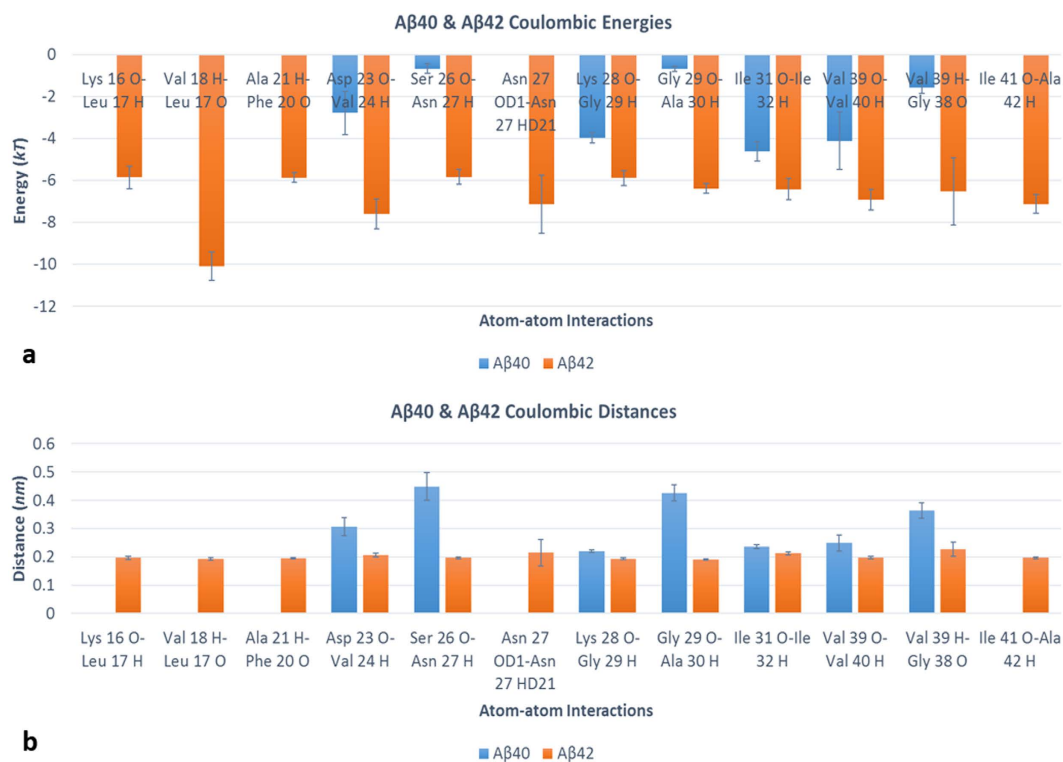


Figure 1. (a,b) Atom-atom interactions imparting exceptionally strong hydrogen bonding energies in the 1:2 configuration of A β 42 compared to A β 40 (a) and their respective atom-atom interaction distances (b) 95% confidence interval error bars included for analysis across all ensemble members. The first three, sixth, and last interactions were not observed in A β 40. Interaction partners are presented as the residue, residue number in the sequence and the residue's atom of one chain (chain A for both strains) interacting with its partner atom in the 1:2 configuration (on the D-chain in A β 40 or on the B-chain in A β 42).

Such a comparative analysis may in turn help to characterize the long-term stability and associated neuronal toxicity of A β 42. Additionally, identifying the underlying key features of the differences of the two strains may provide insight into new therapeutic approaches to inhibit A β 42 aggregation formation. We therefore attempt to identify and characterize the underlying behavior of inter-peptide chain non-covalent interactions by carrying out detailed atomic level energy mappings for both A β 40 and A β 42 mature fibril structures. In doing so, we aim to answer the following two questions: (1) What are the key differences in the inter-chain interaction energetic profiles of A β 40 fibrils and A β 42 fibrils? and (2) What are the underlying conformational changes that are responsible for these differences?

Results

For our study, we initially analyzed and compared the fibril structures of A β 40 (PDB ID: 2M4J by Lu *et al.*³⁶) and A β 42 (PDB ID: 2MXU by Xiao *et al.*³²) according to the Coulombic (charge and partial atomic charge) and Lennard-Jones (Born and van der Waals forces) atom-atom interaction forces as laid out in the open-source

| | A β 40 (A-G) | A β 42 (A-C) |
|----------------------------------------|--------------------|--------------------|
| Coulombic Interactions: | 19 | 36 |
| Coulombic Average E (<i>kT</i>): | -0.352 ± 0.004 | -0.398 ± 0.003 |
| Coulombic Average D (nm): | 0.892 ± 0.006 | 0.877 ± 0.004 |
| Lennard-Jones Interactions: | 0 | 0 |
| Lennard-Jones Average E (<i>kT</i>): | 0 | 0 |
| Lennard-Jones Average D (nm) | 0 | 0 |

Table 2. Comparison of the quantity of the number of dominant atom-atom interaction pairs, average energy (per interaction pair) and average inter-atomic distance (per interaction pair) of 1:3 atom-atom interactions between two chains for A β 40 (A-G chain mapping results) and A β 42 (A-C chain mapping results) with 95% confidence intervals for analysis across all ensemble members. Energy units are in *kT* and distance units are in nanometers.

| Atom-atom Interaction Pairs | | Secondary Structure Acquired in A β 42 Interaction Pairs | |
|-----------------------------|-----------------------------------------------------|----------------------------------------------------------------|------------------------------------|
| A Chain | Partner Chain: D (A β 40) or B (A β 42) | A Chain Residue (A β 42) | B Chain Residue (A β 42) |
| Ser 26 O | Asn 27 H | β -sheet increase | β -sheet increase |
| Asp 23 O | Val 24 H | Left-hand α -helix increase | β -sheet increase |
| Gly 29 O | Ala 30 H | Left-hand α -helix increase | No change |
| Lys 28 O | Gly 29 H | No change | Left-hand α -helix increase |
| Ile 31 O | Ile 32 H | β -sheet decrease | β -sheet increase |
| Val 39 O | Val 40 H | No change | β -sheet increase |
| Val 39 H | Gly 38 O | No change | β -sheet increase |

Table 3. Secondary structure motifs that are more well-defined in A β 42 compared to A β 40.

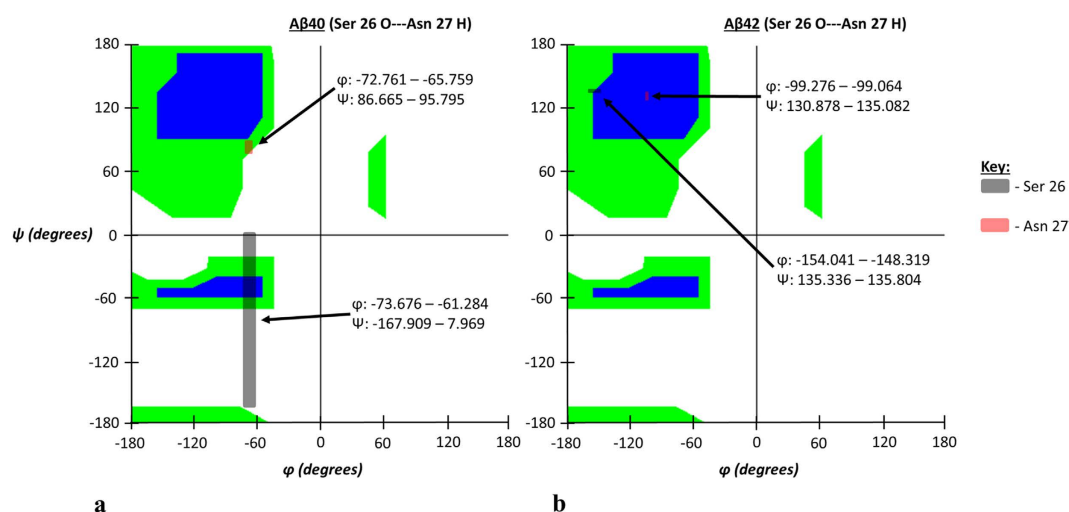


Figure 2. (a,b) Ramachandran angle profiles for an exceptionally strong atom-atom interaction (Ser 26 O interacting with Asn 27 H) for A β 40 (a) and A β 42 (b). Ranges for ϕ and ψ correspond to data spread according to 95% confidence interval analysis for all ensemble members as previously described. As stated before, the first atom is from the A chain of both isoforms and the second corresponds to the partner atom on the appropriate 1:2 interaction chain configuration. Note noticeable increase in β -sheet Ramachandran angle values for both residues of A β 42.

energy mapping algorithm developed by Krall, Brunn, Kankanala and Peters³⁷. This mapping algorithm efficiently parses the strongest non-covalent atom-atom interactions and their inter-atomic distances from structure file data according to empirically established criteria based on the AMBER 03 force field model to ensure that all dominant interactions are accounted for^{37–39}. Those parsing criteria were taken as the upper limit of -0.1 *kT* units for Lennard-Jones criteria and -0.3 *kT* units for Coulombic interactions³⁷. The A β 40 PDB structure file was composed of three A β 40 peptide stacks, each stack containing three A β 40 peptide chains, arranged in a triangular

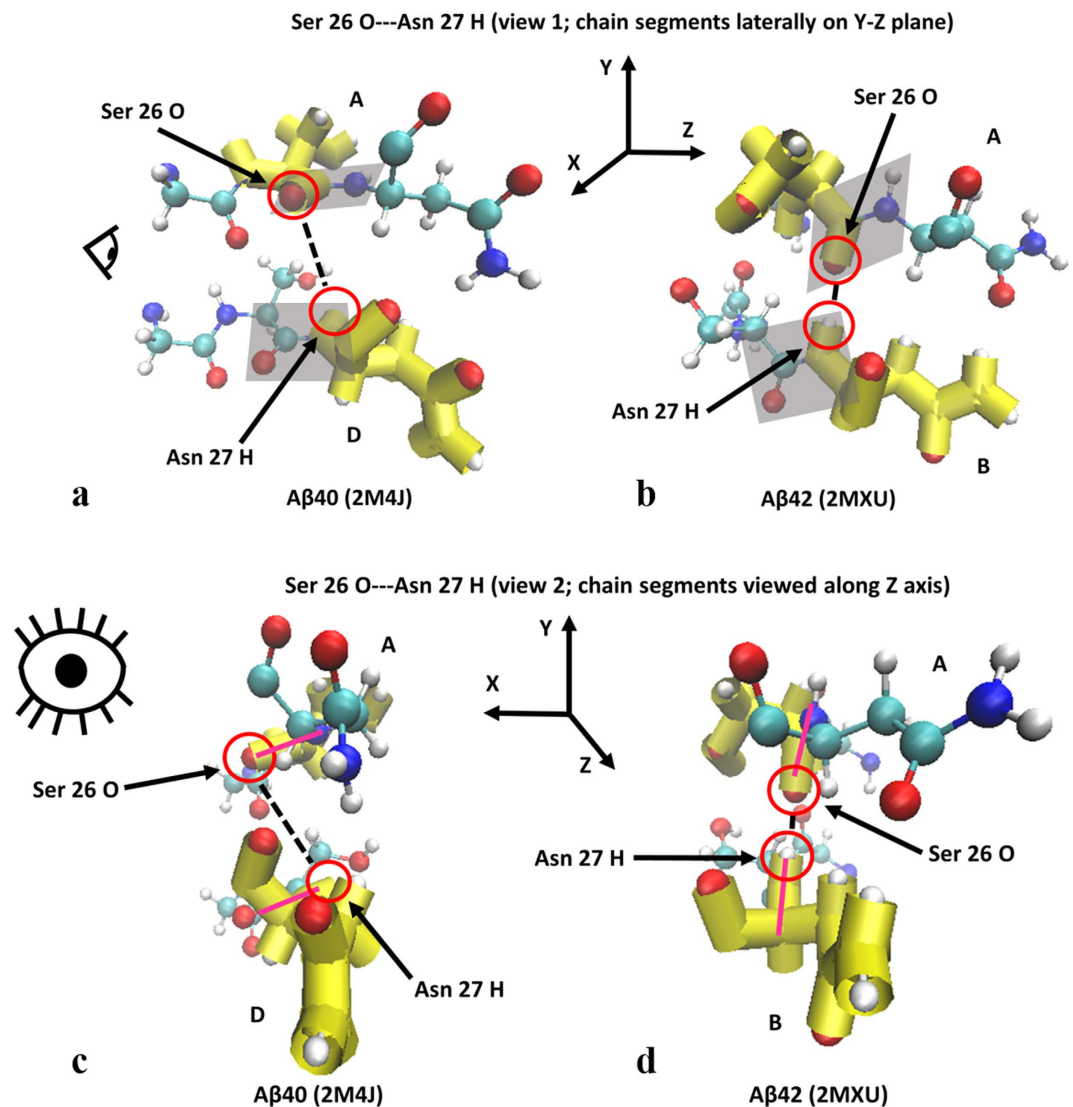


Figure 3. (a–d) Molecule representations of peptide plane alignment for Aβ40 (a,c) and Aβ42 (b,d). Shaded parallelograms in (a,b) are the peptide planes for the residues whose atoms are participating in the hydrogen bonding. (c,d) correspond to a view down the peptide bonds showing the peptide plane profile orientation in magenta. Eye icons indicate view perspective.

three-fold symmetry³⁶ whereas the Aβ42 structure was comprised of only one stack possessing twelve Aβ42 peptide chains³². These two published structures were selected for our analysis due to the fact that they are believed to represent the *in vivo* forms of mature fibrils^{32,36}; very recently, two additional structures of mature Aβ42 fibrils have also appeared (PDB ID: 2NAO by Walti *et al.*⁴⁰ and PDB ID: 5KK3 by Colvin *et al.*⁴¹), which are analyzed and compared following the present analysis of 2MXU. Given the ensemble nature of the structure data for both isoforms, the mapping results for each ensemble member were averaged to obtain the data reported here in the form of 95% confidence intervals for each isoform (questions on how we specifically processed the data files can be directed to the corresponding author). For the Aβ40 structure, we found the results of our energy mappings for each stack to be virtually identical, deviating by only a few percent. Thus, we present the data of the A-D-G stack as representative for what we observed for the entire Aβ40 isoform. Our energy mappings thus involved the investigation of any two inter-chain interaction configurations within one Aβ peptide chain stack: 1) mapping the atom-atom interactions between consecutive/vicinal chains (1:2 interactions) and 2) mapping the atom-atom interactions between non-vicinal chains (1:3 interactions, 1:4, etc...). We also note that, within each isoform, the mapping results between any 1:2, 1:3, etc... chain interactions in the fibril structures were virtually identical to the results of other 1:2, 1:3, etc... interaction systems in the respective fibril structure; so, we report the results for the mapping of the first two chains of each isoform as representative data for their respective strains (mapping chains A-D and A-G for 1:2 and 1:3 interactions respectively for Aβ40 and mapping chains A-B and A-C for 1:2 and 1:3 interactions respectively for Aβ42). The results of the energy mappings found that the Aβ42 isoform has appreciably stronger inter-chain atom-atom interaction binding energies and smaller inter-atomic distances than Aβ40 for both 1:2 and 1:3 interactions thus implying its superior aggregate stability. Interestingly, we observed that

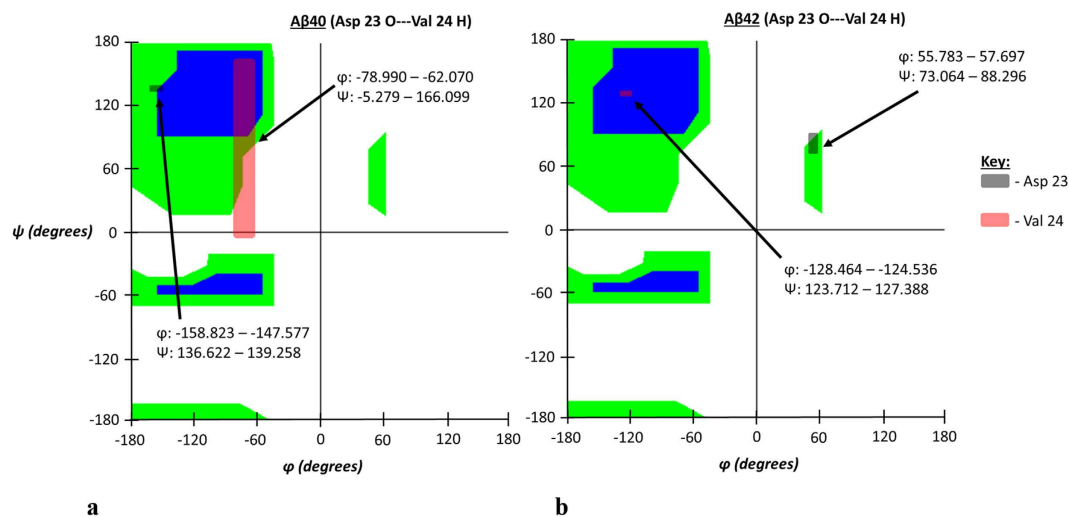


Figure 4. (a,b) Ramachandran angle profiles for an exceptionally strong atom-atom interaction (Asp 23 O interacting with Val 24 H) for A β 40 (a) and A β 42 (b). Ranges for ϕ and ψ correspond to data spread according to 95% confidence interval analysis for all ensemble members as previously described. As stated before, the first atom is from the A chain of both isoforms and the second corresponds to the partner atom on the appropriate 1:2 interaction chain configuration. Note noticeable increase in left-handed α -helix and β -sheet Ramachandran angle values for Asp 23 and Val 24 respectively in the A β 42 isoform.

for the 1:2 interactions, despite A β 42 having stronger inter-chain atom-atom interactions, the quantity of those interactions for that isoform were fewer in number than the quantity of atom-atom interactions observed in the A β 40 isoform. These results are summarized in Table 1 for A β 40 compared against A β 42.

As can be seen, the magnitude of both Coulombic and Lennard-Jones interactions are statistically distinct between the two isoforms according to a 95% confidence interval analysis (i.e. the intervals do not overlap) thus showing that the two strains are energetically different from each other in their inter-chain interaction profiles. Coulombic type interactions were further found to dominate as the primary force for either fibril which stabilizes both strains' infrastructure (Coulombic force interactions being up to 3 to 4 times greater in magnitude than Lennard-Jones interactions). As is widely recognized in the literature, hydrogen bonds were observed to be the greatest constituent contributor to the Coulombic interactions^{29,30} holding the 1:2 chain configuration together for both A β 40 and A β 42 and they were observed to be primarily from backbone carbonyl oxygens and amino hydrogens from the same residues in both strains as discussed in more detail below.

Looking at the longer-range 1:3 interactions, we found that the A β 42 isoform likewise exhibited stronger overall interactions and smaller atom-atom separation distances than A β 40. Unlike the 1:2 interactions, however, all of these 1:3 interactions were exclusively composed of Coulombic atom-atom interactions. No Lennard-Jones interactions were observed for the 1:3 configuration in either fibril. This data is summarized in Table 2.

Like the 1:2 interactions, the observed average energies were statistically different for each isoform. Unlike the 1:2 interactions, however, the stronger bound A β 42 has a superior number of strong atom-atom interactions in addition to a superior average energy per interaction pair for those interactions. An additional noteworthy distinction is that the 1:3 non-vicinal interactions for both strains are not stabilized by hydrogen bonds, but rather carbonyl carbon atoms interacting with carbonyl oxygen atoms serve as the main long-range inter-chain-stabilizing interacting atoms. This is in contrast to the hydrogen bond-rich scenario that marks the 1:2 interactions. No dominant interactions beyond 1:3 interactions (1:4 and up) were observed for either strain. A complete listing of the 1:2 configuration atom-atom pair interaction data is provided as Supplementary Table 1a,b (A β 40 Coulombic and Lennard-Jones interactions respectively) and Supplementary Table 2a,b (A β 42 Coulombic and Lennard-Jones interactions respectively). 1:3 interaction data are in Supplementary Tables 3 and 4.

Due to the fact that the dominant atom-atom interactions involved nearly identical residues in both A β 40 and A β 42 and that the overall average atom-atom distances were smaller in A β 42 (Tables 1 and 2), we postulated that the differences observed for the stronger A β 42 were due to a reduced distance between a smaller set of key interacting atoms in that isoform. Statistical data in the form of 95% confidence intervals for the average distance of the mapping results for both isoforms indeed revealed that the distances were statistically distinct between the two strains for both 1:2 and 1:3 interactions (see Tables 1 and 2). This motivated us to identify those atom-atom interactions, and their corresponding residues, that were primarily responsible for the changes in interacting energies that marked A β 42's superior aggregation interaction stabilities. We note that the strongest 1:2 interaction inter-atomic hydrogen bonds of A β 40 had energy potential values within -4 to -5 kT whereas A β 42's hydrogen bond energy values exhibited a range between -6 to -10 kT for these vicinal chain energy mappings (mapping results for each isoform in Supplementary Table 1a,b and Supplementary Tables 2a,b). From these results of the mapping analysis, we identified 12 atom-atom interaction pairs spanning residues between Lys 16 to Ala 42 that imparted the aforementioned exceptionally strong hydrogen bonds observed throughout the 1:2 chain configuration for A β 42. These residues were identified as those engaging in the exceptionally strong atom-atom interaction

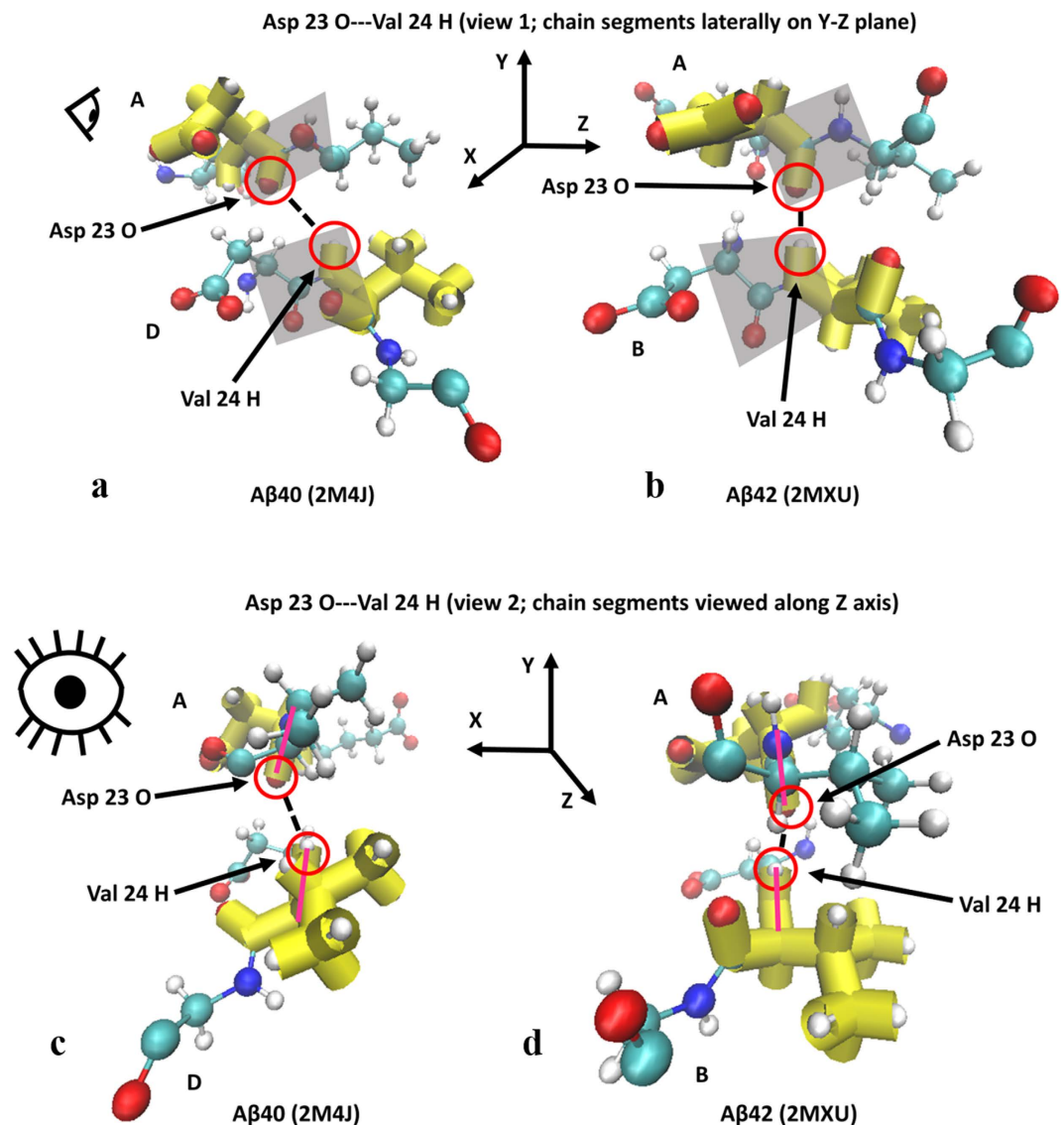


Figure 5. (a–d) Molecule representations of peptide plane alignment for $A\beta 40$ (a,c) and $A\beta 42$ (b,d). Shaded parallelograms in (a,b) are the peptide planes for the residues whose atoms are participating in the hydrogen bonding. (c,d) correspond to a view down the peptide bonds showing the peptide plane profile orientation in magenta. Eye icons indicate view perspective.

pairs that were found in the -6 to -10 kT range for $A\beta 42$ which marked that isoform's unique interaction energy profile. Seven of those 12 interactions involved the same atom-atom pairs in the $A\beta 40$ strain, but their magnitudes in $A\beta 40$ were noticeably weaker. These residues' interactions, their average Coulombic energies and average inter-atomic distances are shown in Fig. 1a,b.

Those interaction energies which were observed in both isoforms were seen to be statistically distinct and considerably weaker in the $A\beta 40$ strain (Fig. 1a) owing to larger inter-atomic distances (Fig. 1b). Interestingly, $A\beta 42$ inter-atomic distances for these exceptionally strong interactions were appreciably uniform unlike those of $A\beta 40$ which showed greater variability. Lastly, we note that for 1:3 interactions, although inter-atomic distances were statistically smaller in $A\beta 42$, atom-atom interaction energy values resided within the same range for both strains ($A\beta 40$ minimum and maximum of -0.3 kT and -0.4 kT respectively vs. $A\beta 42$ minimum and maximum of -0.3 kT and -0.5 kT respectively) indicating that $A\beta 42$'s superior 1:3 interaction strength is owed to a greater number of uniform interactions instead of any single interactions of exceptional energy as was seen in the 1:2 configuration (1:3 interaction mapping results for $A\beta 40$ are in Supplementary Table 3 and 1:3 interaction mapping data for $A\beta 42$ are in Supplementary Table 4).

In light of these findings, we next sought to identify the detailed atomic configurational reasons for the reduced inter-atomic distances of the homologous residues and associated atom-atom interactions seen in the 1:2 configuration's exceptionally strong interactions; it was natural, therefore, to investigate the Ramachandran angle (φ and ψ) differences. The seven exceptionally strong atom-atom interaction pairs that were in both $A\beta 40$ and $A\beta 42$ were found to have φ and ψ angles that oriented the peptide planes more vertically in the $A\beta 42$ isoform which

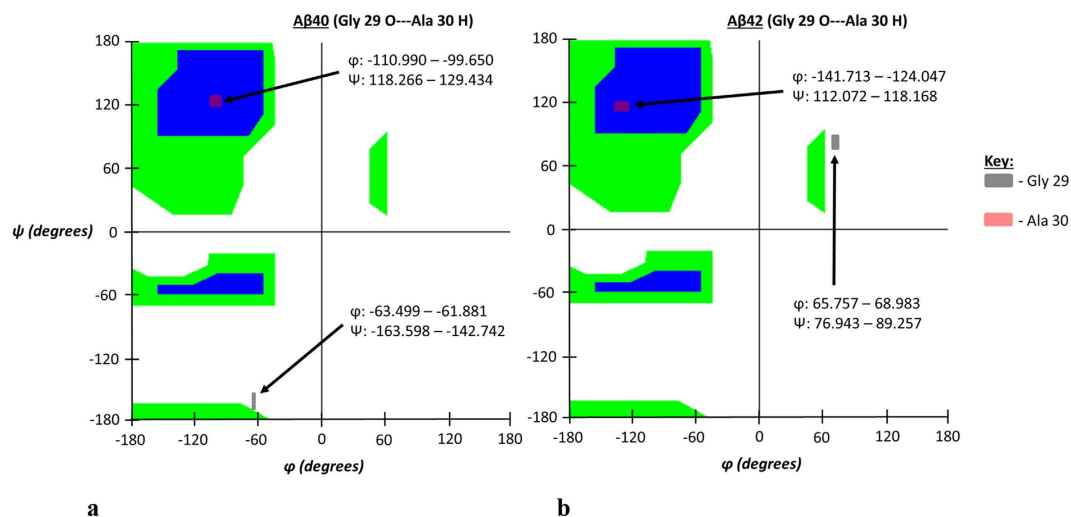


Figure 6. (a,b) Ramachandran angle profiles for an exceptionally strong atom-atom interaction (Gly 29 O interacting with Ala 30 H) for A β 40 (a) and A β 42 (b). Ranges for ϕ and ψ correspond to data spread according to 95% confidence interval analysis for all ensemble members as previously described. As stated before, the first atom is from the A chain of both isoforms and the second corresponds to the partner atom on the appropriate 1:2 interaction chain configuration. Note left-handed α -helix Ramachandran angle values for Gly 29 and the retention of β -sheet Ramachandran angle values for Ala 30 in A β 42 compared to A β 40.

consequently placed the backbone carbonyl oxygen and amino hydrogen atoms closer to each other. Overall, two particular observations are of note for the observed Ramachandran angles: 1) the A β 42 strain shows more well-defined secondary structure primarily favoring β -sheet or left-handed α -helix regions on the Ramachandran plot and 2) the spread of ϕ and ψ angle values tends to be significantly reduced in A β 42. A summary of these more well-defined secondary structure motifs acquired in A β 42's seven exceptionally strong interactions are shown in Table 3.

Additionally, the ϕ and ψ values proved to be statistically unique between the two isoforms thus illustrating distinctiveness between the two structures (complete ϕ and ψ angle data is in Supplementary Table 5). Ramachandran angle changes for three representative interactions are depicted in the figures for the following discussion on these results. The remaining interaction illustrations and Ramachandran angle data are found in Supplementary Fig. 1a,b through Supplementary Fig. 8a–d.

This particular interaction shows the Ramachandran angle values for the A β 42 isoform to clearly reside in β -sheet territory compared to A β 40 thus showing the increased secondary structure characteristics of A β 42 that favor the β -sheet motif for both interacting residues. The resulting changes in peptide plane orientations for the interaction shown in Fig. 2a,b are further depicted in Fig. 3a–d for different viewing perspectives.

As can be seen in Fig. 3, the carbonyl oxygen and amino hydrogen that are involved in the hydrogen bond are considerably closer to each other in the A β 42 isoform thus illustrating that the cause of reduced inter-atomic distances is indeed a vertically-oriented peptide plane. Two additional interactions are presented below that further illustrate this behavior in Ramachandran angles and their effects on peptide plane orientations.

Like the first atom-atom interaction case shown in Fig. 2a,b, the secondary structure of the interaction pair illustrated in Fig. 4a,b shows much more defined secondary structure in the A β 42 strain compared to A β 40. Unlike the preceding case, however, each residue takes on a different secondary structure motif, either left-handed α -helix (Asp 23) or β -sheet (Val 24) as summarized in Table 3. Such differing structure motifs are interesting given the proximal nature of these two residues relative to the primary sequence. Despite the differences in secondary structure characteristics assumed by the interacting residues of A β 42 for this interaction, the peptide planes of the participant atoms were likewise more vertical in the A β 42 isoform as was also seen in the preceding case. This orientation likewise contributed to decreased atom-atom interaction distances and therefore results in the stronger hydrogen bonding observed in that isoform. Images for these peptide plane configurations are shown in Fig. 5a–d.

Although the atoms involved in this example did not show as exaggerated vertical orientation of the peptide planes in the A β 42 strain, inter-atomic distance is nonetheless reduced in that isoform which corresponded to the observed superior interaction energy for this atom-atom pair interaction. For hydrogen bond Coulombic interactions, given the mathematical inverse relationship between the inter-atomic interacting energies and their inter-atomic distances, any appreciable increases in the interaction energy due to reduced distances, however small, are understandable and mathematically expected.

We lastly present a final case where secondary structure was more well-defined in the A β 42 isoform but for only one residue as opposed to both as has been seen in the previous two cases. Ramachandran plots for the respective angles of both A β 40 and A β 42 are shown in Fig. 6a,b.

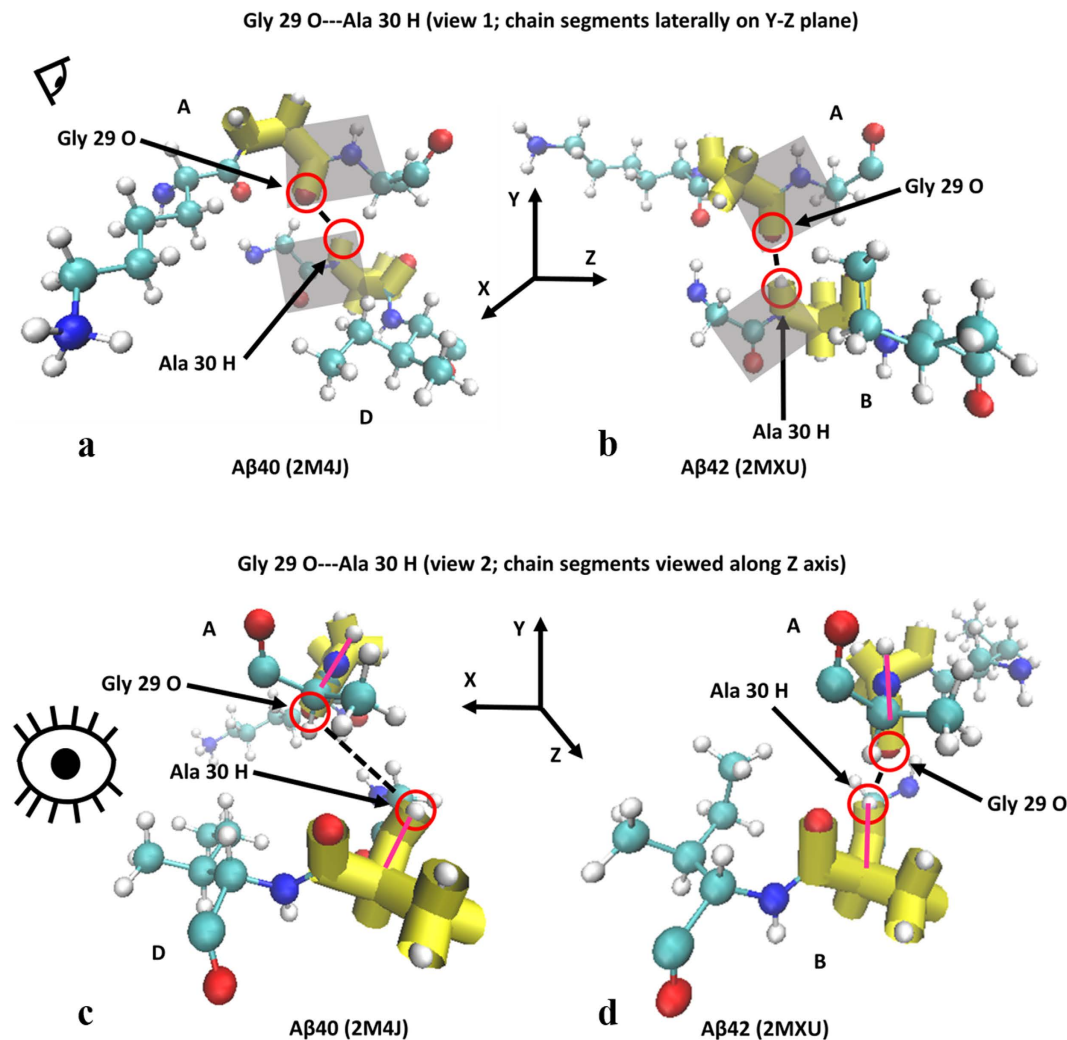


Figure 7. (a–d) Molecule representations of peptide plane alignment for A β 40 (a,c) and A β 42 (b,d). Shaded parallelograms in (a,b) are the peptide planes for the residues whose atoms are participating in the hydrogen bonding. (c,d) correspond to a view down the peptide bonds showing the peptide plane profile orientation in magenta. Eye icons indicate view perspective.

In spite of the variation for the types of secondary characteristics acquired in the A β 42 isoform observed from case to case, the main motif of A β 42 possessing more vertical peptide planes (and hence reduced inter-atomic distances) remained true to this case as well as can be seen in Fig. 7a–d.

Although specific attributes regarding acquired secondary characteristics in the A β 42 strain are observed to vary from different interaction cases, the increased inter-chain interaction strength and stability of the A β 42 fibrils, compared to A β 40 fibrils, can confidently be attributed to Ramachandran angular changes that favor atom orientations that reduce key atom-atom interaction distances. These reduced distances thus favor strong attractive atom-atom interactions (particularly hydrogen bonding) between neighboring chains which appear to result in the superior aggregation stabilities and propensities observed in the A β 42 fibril isoform.

Recently, two additional structures of A β 42 aggregates have been published (PDB ID: 2NAO by Walti *et al.*⁴⁰ and 5KK3 by Colvin *et al.*⁴¹) that allow more comprehensive inter-chain interaction comparisons between A β 42 and A β 40 across independently published structure files. As described below, nearly identical conformational attributes noted above for the A β 42 structure by Xiao *et al.*³² (PDB ID: 2MXU) also occur for these two newly available structure files. Both 2NAO and 5KK3 were comprised of two stacks, but each structure's energy mappings were virtually identical for both stacks so representative data for one stack (the A-C and A-I stacks for 2NAO and 5KK3 respectively) is provided below.

In the case of 2NAO (for the A-B chain interactions) by Walti *et al.*⁴⁰, we found that the average energy per atom-atom interaction pair and the average distance, likewise per atom-atom interaction pair, were -0.828 ± 0.010 *kT* and 0.558 ± 0.002 *nm* respectively. This compares as appreciably similar to the results we obtained for 2MXU's average inter-atomic energy and distance of -0.819 ± 0.008 *kT* and 0.568 ± 0.001 *nm* respectively. This comparative analysis between these two A β 42 structures also led to our observing similar results for 2NAO concerning that structure's β -sheet characteristics likewise reported by Walti *et al.*⁴⁰. Those

residues we identified as contributing to the strongest inter-chain hydrogen bond energies for 2NAO (which also possessed more well-defined secondary structure characteristics through our Ramachandran plot analysis), were also identified as key β -sheet residues by Walti *et al.*'s⁴⁰ experimental chemical shift data. A complete comparison between 2MXU and 2NAO following our above analysis for the 2MXU structure can be found in the Supplemental Information.

In the case of 5KK3 (for the A-B chain interactions) by Colvin *et al.*⁴¹, concurrently, we found that the results were likewise similar to the 2MXU structure. Average energy and distance data per atom-atom interaction pair for 5KK3 were $-0.889 \pm 0.009 kT$ and $0.544 \pm 0.002 nm$ respectively compared to 2MXU's -average energy and distance data of $0.819 \pm 0.008 kT$ and $0.568 \pm 0.001 nm$ respectively. As with the study by Walti *et al.*⁴⁰ for 2NAO, Colvin *et al.*⁴¹ also determined β -sheet structure regions using chemical shift data for their A β 42 fibril structure. Our energetic analysis likewise yielded the identification of the same key residues involved in β -sheet structure as Colvin *et al.*'s⁴¹ chemical shift data. The full analysis data for our comparison of 5KK3 and 2MXU is found in the Supplemental Information.

Discussion

A β 42 is known to engage in persistent aggregation structures more readily than A β 40, but until now, the details of why this is the case have not been clear. Our studies have indicated, however, that the underlying reason behind increased aggregation attractive interactions and their corresponding superior attractive energies in mature A β 42 fibrils is due to a more vertical orientation of peptide planes within each constituent chain that places backbone carbonyl oxygens and amino hydrogens in closer proximity to each other as evidenced by Ramachandran angle data. This consequently allows distance-dependent non-covalent attractive interaction energies in the form of hydrogen bonds to flourish in A β 42 which results in that isoform's stronger inter-chain interactions compared to the weaker A β 40 strain. Additionally, Ramachandran angles of A β 42 peptide chains in the fibril structure indicate that A β 42 has more well-defined secondary structure characteristics (specifically, β -sheet and left-handed α -helix) compared to A β 40. Indeed, the importance of Ramachandran angle changes have even been observed in the study of aggregation transition from pre-fibrillar aggregate structures to mature fibrils^{42,43}.

A natural follow-up inquiry to these observations would then seek to probe the reason(s) why the A β 42 strain adopts more vertical peptide plane configurations. We postulate that, given A β 42's additional two C-terminal residues (Ile 41 and Ala 42), individual A β 42 peptide chains are perhaps able to sample fold-like configurations in the early aggregation process that allow Ramachandran angles which permit the more vertical peptide planes that favor stronger hydrogen bonding attractive interaction energies. Given A β 40's lack of these two C-terminal residues, it, by contrast, may perhaps not favorably sample those same conformations that favor reduced inter-atomic distances. Indeed, Urbanc *et al.*⁴⁴ discerned differences in the conformations assumed by monomer peptides of A β 40 and A β 42 during their computational simulation of the actual aggregation process for both isoforms. Such differences between isoforms observed during aggregation growth may yet be observed in the range of individual monomer motion preceding the actual aggregation process when considering the potential effects on individual monomer movement imparted by the last two C-terminal residues in A β 42. Ultimately, therefore, the phenomenon behind A β 42's superior attractive interactions and superior stability, may be traced to concepts in the protein folding problem as they pertain to the three-dimensional configurations both isoforms' monomers distinctively sample prior to the early aggregation/oligomer stages leading up to mature fibril formation.

References

1. Annaert, W. & De Strooper, B. A cell biological perspective on Alzheimer's disease. *Annual review of cell and developmental biology* **18**(1), 25–51 (2002).
2. LaFerla, F. M., Green, K. N. & Oddo, S. Intracellular amyloid- β in Alzheimer's disease. *Nature Reviews Neuroscience* **8**(7), 499–509 (2007).
3. Selkoe, D. J. Alzheimer's disease: genes, proteins, and therapy. *Physiological reviews* **81**(2), 741–766 (2001).
4. Selkoe, D. J. Cell biology of protein misfolding: the examples of Alzheimer's and Parkinson's diseases. *Nature cell biology* **6**(11), 1054–1061 (2004).
5. Klafki *et al.* Validation of a commercial chemiluminescence immunoassay for the simultaneous measurement of three different amyloid- β peptides in human cerebrospinal fluid and application to a clinical cohort. *Journal of Alzheimer's Disease* (Preprint), 1–15 (2016).
6. Davis, J. & Van Nostrand, W. E. Enhanced pathologic properties of Dutch-type mutant amyloid beta-protein. *Proceedings of the National Academy of Sciences* **93**(7), 2996–3000 (1996).
7. Davis-Salinas, J., Saporito-Irwin, S. M., Cotman, C. W. & Van Nostrand, W. E. Amyloid β -protein induces its own production in cultured degenerating cerebrovascular smooth muscle cells. *Journal of neurochemistry* **65**(2), 931–934 (1995).
8. Luheshi, L. M. *et al.* Systematic *in vivo* analysis of the intrinsic determinants of amyloid β pathogenicity. *PLoS Biol* **5**(11), e290 (2007).
9. Murakami, K. *et al.* Neurotoxicity and physicochemical properties of A β mutant peptides from cerebral amyloid angiopathy implication for the pathogenesis of cerebral amyloid angiopathy and Alzheimer's disease. *Journal of Biological Chemistry* **278**(46), 46179–46187 (2003).
10. Bitan, G. *et al.* Amyloid β -protein (A β) assembly: A β 40 and A β 42 oligomerize through distinct pathways. *Proceedings of the National Academy of Sciences* **100**(1), 330–335 (2003).
11. Gong, Y. *et al.* Alzheimer's disease-affected brain: presence of oligomeric A β ligands (ADDLs) suggests a molecular basis for reversible memory loss. *Proceedings of the National Academy of Sciences* **100**(18), 10417–10422 (2003).
12. Mastrangelo, I. A. *et al.* High-resolution atomic force microscopy of soluble A β 42 oligomers. *Journal of molecular biology* **358**(1), 106–119 (2006).
13. Ahmed, M. *et al.* Structural conversion of neurotoxic amyloid-[beta] 1-42 oligomers to fibrils. *Nature structural & molecular biology* **17**(5), 561–567 (2010).
14. Walsh, D. M. *et al.* Naturally secreted oligomers of amyloid β protein potently inhibit hippocampal long-term potentiation *in vivo*. *Nature* **416**(6880), 535–539 (2002).
15. Dahlgren, K. N. *et al.* Oligomeric and fibrillar species of amyloid- β peptides differentially affect neuronal viability. *Journal of Biological Chemistry* **277**(35), 32046–32053 (2002).

16. Chimon, S. *et al.* Evidence of fibril-like β -sheet structures in a neurotoxic amyloid intermediate of Alzheimer's β -amyloid. *Nature structural & molecular biology* **14**(12), 1157–1164 (2007).
17. Petkova, A. T. *et al.* Self-propagating, molecular-level polymorphism in Alzheimer's β -amyloid fibrils. *Science* **307**(5707), 262–265 (2005).
18. Qiang, W., Yau, W. M., Luo, Y., Mattson, M. P. & Tycko, R. Antiparallel β -sheet architecture in Iowa-mutant β -amyloid fibrils. *Proceedings of the National Academy of Sciences* **109**(12), 4443–4448 (2012).
19. Walsh, D. M. *et al.* Amyloid β -protein fibrillogenesis structure and biological activity of protofibrillar intermediates. *Journal of Biological Chemistry* **274**(36), 25945–25952 (1999).
20. Knowles, T. P., Vendruscolo, M. & Dobson, C. M. The amyloid state and its association with protein misfolding diseases. *Nature reviews Molecular cell biology* **15**(6), 384–396 (2014).
21. Knowles, T. P. *et al.* An analytical solution to the kinetics of breakable filament assembly. *Science* **326**(5959), 1533–1537 (2009).
22. Collins, S. R., Dougllass, A., Vale, R. D. & Weissman, J. S. Mechanism of prion propagation: amyloid growth occurs by monomer addition. *PLoS Biol* **2**(10), e321 (2004).
23. Mucke, L. *et al.* High-level neuronal expression of A β 1–42 in wild-type human amyloid protein precursor transgenic mice: synaptotoxicity without plaque formation. *The Journal of neuroscience* **20**(11), 4050–4058 (2000).
24. Deshpande, A., Mina, E., Glabe, C. & Busciglio, J. Different conformations of amyloid β induce neurotoxicity by distinct mechanisms in human cortical neurons. *The Journal of neuroscience* **26**(22), 6011–6018 (2006).
25. Lührs, T. *et al.* 3D structure of Alzheimer's amyloid- β (1–42) fibrils. *Proceedings of the National Academy of Sciences of the United States of America* **102**(48), 17342–17347 (2005).
26. Olofsson, A., Sauer-Eriksson, A. E. & Öhman, A. The solvent protection of Alzheimer amyloid- β -(1–42) fibrils as determined by solution NMR spectroscopy. *Journal of Biological Chemistry* **281**(1), 477–483 (2006).
27. Masuda, Y. *et al.* Identification of physiological and toxic conformations in A β 42 aggregates. *ChemBioChem* **10**(2), 287–295 (2009).
28. Sakono, M. & Zako, T. Amyloid oligomers: formation and toxicity of A β oligomers. *FEBS journal* **277**(6), 1348–1358 (2010).
29. Petkova, A. T. *et al.* A structural model for Alzheimer's β -amyloid fibrils based on experimental constraints from solid state NMR. *Proceedings of the National Academy of Sciences* **99**(26), 16742–16747 (2002).
30. Sunde, M. *et al.* Common core structure of amyloid fibrils by synchrotron X-ray diffraction. *Journal of molecular biology* **273**(3), 729–739 (1997).
31. Inouye, H., Fraser, P. E. & Kirschner, D. A. Structure of beta-crystallite assemblies formed by Alzheimer beta-amyloid protein analogues: analysis by x-ray diffraction. *Biophysical journal* **64**(2), 502–519 (1993).
32. Xiao, Y. *et al.* A [beta](1–42) fibril structure illuminates self-recognition and replication of amyloid in Alzheimer's disease. *Nature structural & molecular biology* **22**(6), 499–505 (2015).
33. Pauwels, K. *et al.* Structural basis for increased toxicity of pathological a β 42: a β 40 ratios in Alzheimer disease. *Journal of biological chemistry* **287**(8), 5650–5660 (2012).
34. Stöhr, J. *et al.* Distinct synthetic A β prion strains producing different amyloid deposits in bigenic mice. *Proceedings of the National Academy of Sciences* **111**(28), 10329–10334 (2014).
35. Nabers, A. *et al.* Amyloid- β -secondary structure distribution in cerebrospinal fluid and blood measured by an immuno-infrared-sensor: A biomarker candidate for Alzheimer's disease. *Analytical Chemistry* **88**(5), 2755–2762 (2016).
36. Lu, J. X. *et al.* Molecular structure of β -amyloid fibrils in Alzheimer's disease brain tissue. *Cell* **154**(6), 1257–1268 (2013).
37. Krall, A., Brunn, J., Kankanala, S. & Peters, M. H. (2014). A simple contact mapping algorithm for identifying potential peptide mimetics in protein–protein interaction partners. *Proteins: Structure, Function, and Bioinformatics* **82**(9), 2253–2262.
38. Peters, M. Force descriptions. In: McCombs, K. P. ed. *Real-Time Biomolecular Simulations*. New York, New York: McGraw Hill; 58–62 (2007).
39. Stöbener, K. *et al.* Multicriteria optimization of molecular force fields by Pareto approach. *Fluid Phase Equilibria* **373**, 100–108 (2014).
40. Walti, M. A. *et al.* Atomic-resolution structure of a disease-relevant abeta(1–42) amyloid fibril. *Proceedings of the National Academy of Sciences of the United States of America* **113**(34), E4976–E4984 (2016).
41. Colvin, M. T. *et al.* Atomic resolution structure of monomorphous A β 42 amyloid fibrils. *Journal of the American Chemical Society* **138**(30), 9663–9674 (2016).
42. Armen R. S., DeMarco M. L., Alonso D. O. & Daggett V. Pauling and Corey's alpha-pleated sheet structure may define the prefibrillar amyloidogenic intermediate in amyloid disease. *Proc Natl Acad Sci USA* **101**(32), 11622–11627 (2004).
43. Milner-White, J. E., Watson, J. D., Qi, G. & Hayward, S. Amyloid formation may involve α -to β sheet interconversion via peptide plane flipping. *Structure* **14**(9), 1369–1376 (2006).
44. Urbanc, B. *et al.* In silico study of amyloid beta-protein folding and oligomerization. *Proceedings of the National Academy of Sciences of the United States of America* **101**(50), 17345–17350 (2004).

Author Contributions

O.B. and M.P. wrote the main manuscript text and B.G. and M.S. assisted with data evaluation and all figure and table preparation.

Additional Information

Supplementary information accompanies this paper at <http://www.nature.com/srep>

Competing financial interests: The authors declare no competing financial interests.

How to cite this article: Bastidas, O. H. *et al.* Few Ramachandran Angle Changes Provide Interaction Strength Increase in A β 42 versus A β 40 Amyloid Fibrils. *Sci. Rep.* **6**, 36499; doi: 10.1038/srep36499 (2016).

Publisher's note: Springer Nature remains neutral with regard to jurisdictional claims in published maps and institutional affiliations..



This work is licensed under a Creative Commons Attribution 4.0 International License. The images or other third party material in this article are included in the article's Creative Commons license, unless indicated otherwise in the credit line; if the material is not included under the Creative Commons license, users will need to obtain permission from the license holder to reproduce the material. To view a copy of this license, visit <http://creativecommons.org/licenses/by/4.0/>

© The Author(s) 2016